Progress In Electromagnetics Research Letters, Vol. 58, 81–88, 2016

Hilbert Curve Fractal Antenna for Dual On- and Off-Body Communication

Susilo Ady Saputro and Jae-Young Chung*

Abstract—We present a Hilbert curve fractal antenna operating at 2.45 GHz ISM and 5.5 GHz WLAN bands. The proposed antenna employs a third-order Hilbert curve and two shorting vias for antenna miniaturization and dual-band/mode operation. At 2.45 GHz, the antenna exhibits a monopole-like radiation pattern, while at 5.5 GHz, it provides a broadside radiation pattern, suitable for simultaneous on- and off-body communication using two distinct frequency bands. The antenna footprint is as small as 25.5 mm × 25.5 mm. Simulation and measurement results demonstrate that the antenna gain is more than 1.9 dBi if the antenna is mounted on a ground larger than 40 mm × 40 mm. The effect of human body presence on antenna performance was investigated by means of full-wave simulations locating the antenna on a human body phantom. It is shown that the proposed antenna is capable of maintaining its free-space performance over the human body phantom except for the gain reduction of 2.5 dBi at 5.5 GHz band.

1. INTRODUCTION

Rapid development in wireless communication technology has brought great attention to Wireless Body Area Network (WBAN) communications. Applications of WBAN can be found in many aspects, such as personal healthcare, sport, entertainment, military and security [1]. There are three main scenarios in WBAN communication links: in-, on- and off-body communications. For the last, an antenna is required to have a broadside radiation pattern perpendicular to the body surface with small backward radiation. For the on-body communication, an antenna with omnidirectional radiation pattern is preferred for efficient communication parallel to the body surface [2]. In order to realize simultaneous off- and on-body communications, it is necessary to design an antenna with pattern diversity capable of generating both the broadside and omnidirectional radiation pattern in a single element. Also, the antenna needs be compact and in low profile to comply with on-body installation.

In previous studies, the pattern diversity is carried out using an additional phase shifter or reactive loading [3, 4]. However, these methods are often not suitable for wearable applications due to their size limitation. To overcome this problem, reconfigurable antennas have been proposed. They offer pattern and frequency diversity by selectively incorporating with a different feeding/antenna pair using electrical switches [5, 6]. But still, difficulties in fabrication remain due to bias lines for turning on/off the switches. On the other hand, Nessel et al. [7] proposed a switchless antenna offering radiation pattern diversity at two separate resonance frequencies. The antenna employs a folded Hilbert curve with a 5 mm × 5 mm footprint and operates at 2.3 GHz (S-band) and 16.8 GHz (Ku-band) with omnidirectional and broadside radiation patterns, respectively.

In this paper, we propose a Hilbert curve fractal antenna with dual-band pattern diversity operating at 2.45 GHz Industrial-Scientific-Medical (ISM) and 5.5 GHz Wireless Local Area Network (WLAN) bands for wearable on- and off-body communications. The antenna is designed to provide

Received 11 November 2015, Accepted 31 December 2015, Scheduled 18 January 2016
* Corresponding author: Jae-Young Chung (jychung@seoultech.ac.kr).
The authors are with the Department of Electrical and Information Engineering, Seoul National University of Science and Technology, Seoul 139-743, Korea.

omnidirectional radiation pattern at 2.45 GHz and broadside radiation pattern at 5.5 GHz. Most of the WBANs utilize the ISM band centered at 2.45 GHz due to its license-free and worldwide availability [8]. However, 2.45 GHz ISM band is prone to coexistence with other standard (i.e., IEEE 802.15.1, IEEE 802.15.4, IEEE 802.11b/g/n), making 5.5 GHz WLAN band a good option for off-body communication since it provides less interference and wider bandwidth. The dual-band impedance matching and dual-mode pattern diversity are implemented by diversifying the current paths at the two bands by shorting the upper layer Hilbert curve to the ground using vias. No electrical or mechanical switches are included, thus making the structure simple and small. Details of the antenna structure and operating mechanism are described in Section 2. Simulation and measurement results of the optimized design are presented in Section 3. In Section 4, body-worn performance of the proposed antenna is investigated and discussed.

2. ANTENNA DESIGN

2.1. Antenna Geometry

High-order space-filling fractal curves are progressively used for antenna miniaturization since they offer compact implementation of a long inductive line [9, 10]. The third-order Hilbert curve is used for the proposed antenna considering the given antenna footprint less than 30 mm × 30 mm. The total length of the Hilbert curve (S) can be calculated by [10]:

$$S = \left(2^{2n} - 1\right) d = \left(2^n + 1\right) L \tag{1}$$

where n is the iteration order, L the length of external dimension, and d the length of each segment corresponding to $d = L/(2^n - 1)$. With the above, the resonance frequency turns out to be 1.45 GHz when the third-order Hilbert curve of length $S = 450$ mm and $L = 50$ mm is used. From this initial value, the antenna is optimized to resonate at 2.45 GHz and 5.5 GHz dual-band by locating shorting vias, adjusting the external length and altering the line widths of each arm.

Figure 1 shows the antenna layout. The Hilbert curve with the total footprint of 15.5 mm × 15.5 mm is printed on a 25.5 mm × 25.5 mm × 1.6 mm Teflon® substrate whose dielectric constant and loss tangent are $\varepsilon_r = 2.2$, $\tan\delta = 0.001$. The antenna is fed by a 50-Ω coaxial probe. The substrate and ground are separated by a 6.35 mm thick air layer, and they are connected with two vias located at arm-1 and -4 [See Figure 1(a)]. Each arm of the Hilbert curve has different width values of 1.45 mm, 1.6 mm, 1.7 mm and 1.2 mm followed by the indices 1 to 4. Such self-affine fractal geometry [11–13] offers more freedom in antenna impedance tuning as demonstrated in the parametric studies.

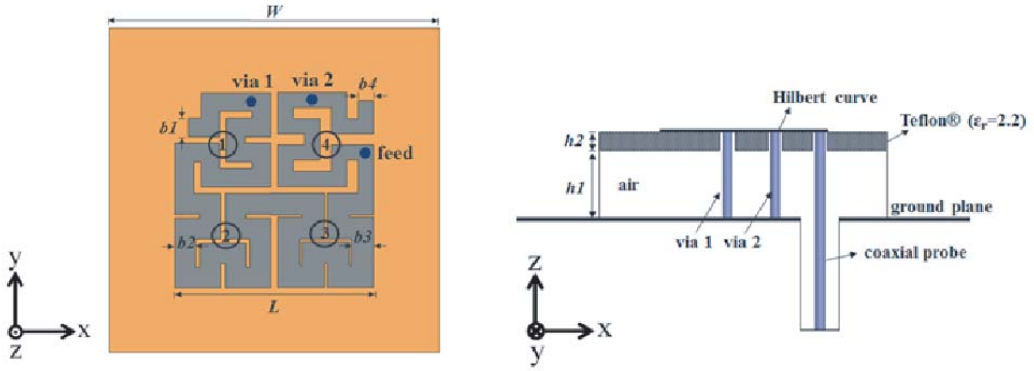

(a) (b)

Figure 1. Layout of the Hilbert curve fractal antenna. (a) Top-view and (b) side view. $W = 25.15$, $L = 15.15$, $b1 = 1.45$, $b2 = 1.6$, $b3 = 1.7$, $b4 = 1.2$, $h1 = 6.35$, $h2 = 1.6$. All units are in millimeter.

2.2. Current Distribution and Radiation Pattern

Figure 2 shows the current distribution at 2.45 GHz and 5.5 GHz. At 2.45 GHz, the currents are distributed over the Hilbert curve arm-1, -3 and via-1. In this state, the antenna operates like a

top-loaded monopole consisting of two radiating elements: the Hilbert curve as the horizontal radiating component and via-1 as the vertical radiating component. The combination of these two generates an omnidirectional radiation pattern with a smaller broadside null than a traditional monopole-like pattern. The shorting via is useful not only for impedance matching as in conventional inverted-F antennas (IFA), but also for generating omnidirectional radiations despite the low-profile configuration. Without the current path along the via, the antenna operates as an ordinary Hilbert curve patch with a broadside radiation pattern. This is the case for Figure 2(b) at 5.5 GHz. It is shown that the currents are mostly distributed on the Hilbert curve instead of the vias. Note that two vias are necessary to attain good impedance matching at the both bands. Also, it is observed that via-1 and via-2 are more responsible for omnidirectional radiation pattern and good impedance matching at the low band, respectively.

2.3. Parametric Studies

Parametric studies based on full-wave simulations show that the antenna performance is affected by key geometrical parameters. Herein, we report the changes in antenna impedance and gain as the width of Hilbert curve and ground size vary. Figure 3(a) presents the S_{11} simulation results by varying the width of arm-1 [See $b1$ in Figure 1(a)]. A step increment of 0.1 mm of $b1$ leads the upper 5.5 GHz band resonant frequency to decrease, while that of the low 2.45 GHz band stays the same. Therefore, a small change in the width of Hilbert arm is trivial for low band but highly affects the high band impedance, especially for strong current flowing on arm-1 and -4 as in Figure 2(b). Figure 3(b) shows the change in S_{11} by altering the width of arm-4 ($b4$). It is seen that the narrower $b4$ results in lower S_{11} with the expense of narrower bandwidth. Based on these trade-offs, we chose $b1 = 1.45$ mm and $b4 = 1.2$ mm in the proposed design.

Figure 4(a) shows S_{11} simulation results by varying the ground size. The overall S_{11} is not influenced as the ground size varies from 40 mm × 40 mm to 100 mm × 100 mm except for slight changes in the

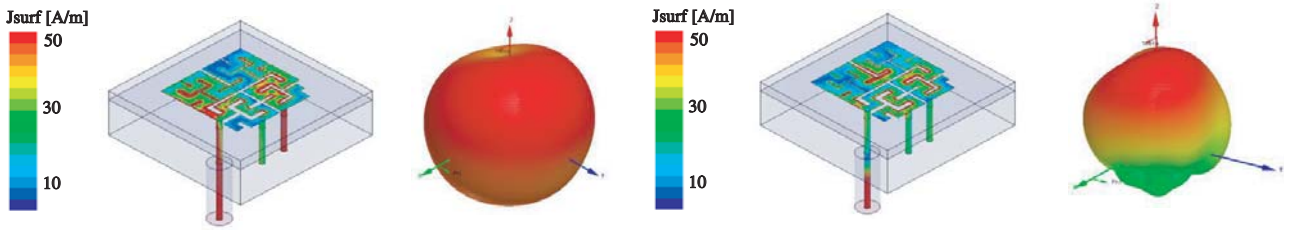

(a) (b)

Figure 2. Simulated current distributions on radiating elements for (a) 2.45 GHz and (b) 5.5 GHz.

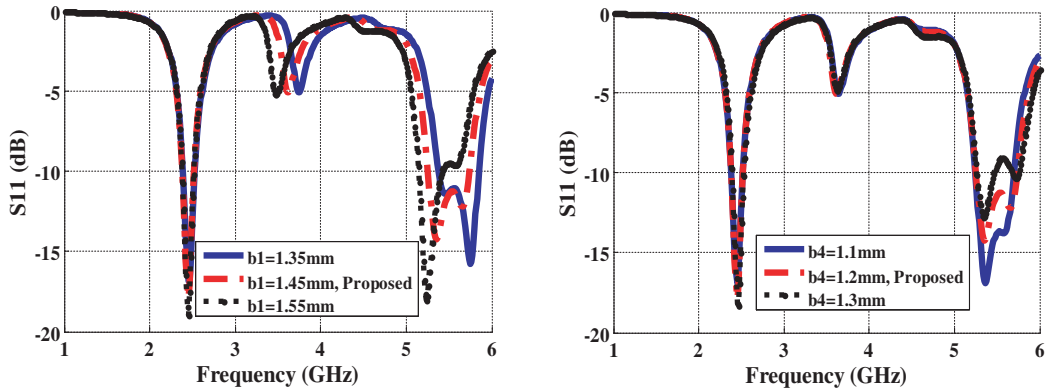

(a) (b)

Figure 3. S_{11} simulation results by varying the width of Hilbert arm: (a) varying $b1$ (upper left arm-1), and (b) varying $b4$ (upper right arm-4).

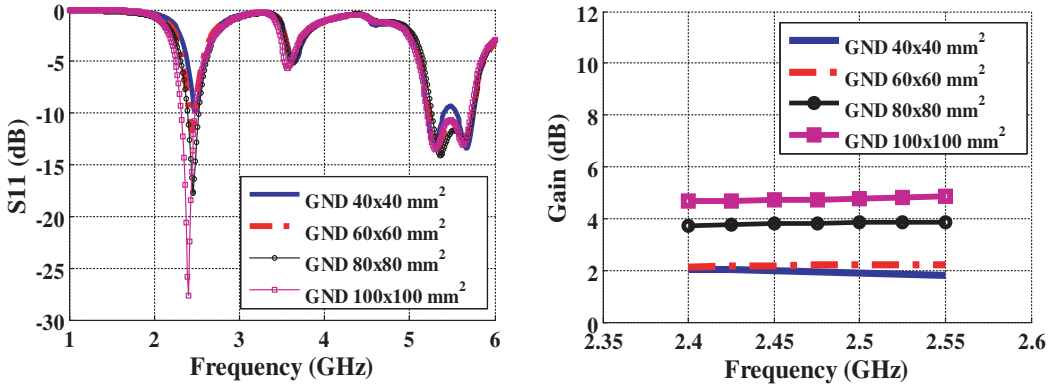

Figure 4. Effects of the ground plane size on (a) S_{11} and (b) antenna gain at 2.45 GHz band.

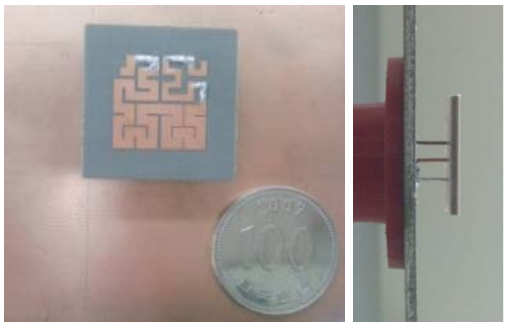

Figure 5. Photograph of proposed antenna fabricated on Teflon® substrate.

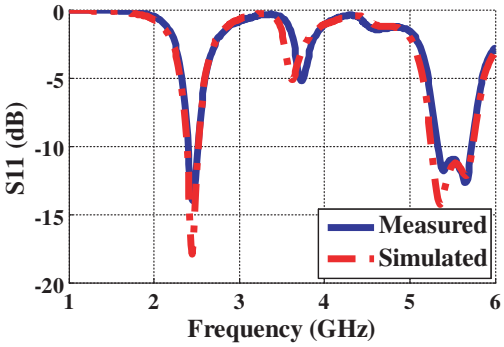

Figure 6. Measurement and simulation results of S_{11}.

low band resonant frequency. Figure 4(b) shows the corresponding gain changes at the 2.45 GHz band. The increase in antenna gain is observed as the larger ground is employed. More specifically, the gain increases from 1.9 to 4.67 dB as the ground extends from 40 mm × 40 mm to 100 mm × 100 mm. In contrast to 2.45 GHz band, antenna gain at 5.5 GHz is insensitive to the changes of ground size. This is due to the fact that most of the currents are concentrated on the Hilbert curve, and only a small amount is distributed on the ground at 5.5 GHz. In addition, we note that the asymmetry between the two opposite arms (i.e., arm-1 and arm-4) is to improve the 5.5 GHz bandwidth. Eroding the upper left part of arm-1 broadens the 5.5 GHz bandwidth without affecting the 2.45 GHz band matching.

3. FABRICATION AND MEASUREMENT

An antenna prototype was fabricated, and its matching and radiation properties were measured by a network analyzer and anechoic chamber. Figure 5 shows pictures of the fabricated prototype. The optimized Hilbert curve design was printed on a Teflon substrate by PCB lamination process. The ground was made from a single-side laminated FR-4 substrate. All the dimensional parameters are identical to those described in Figure 1. Figure 6 shows the measured S_{11} on top of the simulation data. A good agreement between the two can be observed. The $S_{11} < -10$ dB bandwidths measured at 2.45 and 5.5 GHz are 112 MHz (4.57%) and 400 MHz (7.27%), respectively.

Figures 7(a) and (b) are the measured radiation pattern in the yz-plane at 2.45 GHz and 5.5 GHz (See the coordinate conventions in Figure 1). For the 2.45 GHz pattern, one can observe a monopole-like pattern with a slight asymmetry between the left and right sides. The latter is caused by the asymmetric shorting vias' locations along the Hilbert curve. The maximum directivity occurs at $\theta = 45°$ due to

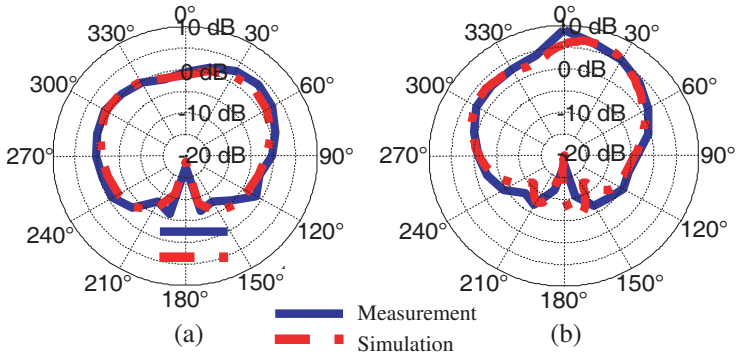

Figure 7. Measured and simulated radiation pattern at (a) 2.45 GHz and (b) 5.5 GHz.

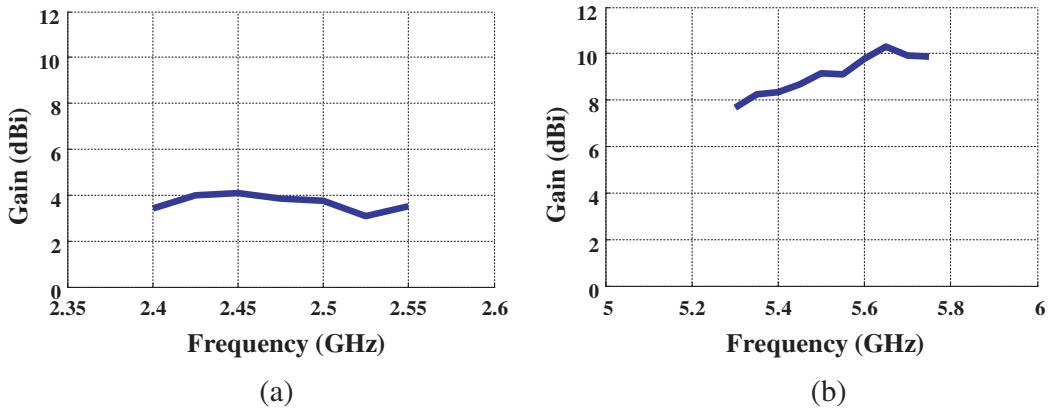

Figure 8. Measured gain of the proposed antenna at (a) 2.45 GHz and (b) 5.5 GHz band.

the ground effect similar to an ordinary $\lambda/4$ monopole antenna. The broadside null is not as deep as a monopole antenna for the reason already mentioned in Section 2. At 5.5 GHz, a typical broadside radiation pattern can be observed. In this context, the proposed antenna can be thought as a good antenna candidate for dual on- and off-body communications utilizing the omnidirectional radiation pattern at 2.45 GHz and broadside pattern at 5.5 GHz, respectively. A much higher gain value is attained for 5.5 GHz than 2.45 GHz band, and this is depicted in Figure 8. In the lower 2.45 GHz band, the measured peak gain varies from 3.4 to 4.1 dBi. As for the higher 5.5 GHz band, the peak gain ranges from 8.25 to 10.28 dBi.

4. BODY-WORN PERFORMANCE

For such a body-worn application, it was critical to investigate the effects of human body presence on antenna performance. Previous studies showed that the impedance matching, gain, radiation pattern can be affected when a wearable antenna is located in the vicinity of a lossy human body [14, 15]. To identify the human body influence on antenna performance, we modeled a three-layer tissue phantom emulating the front abdomen of human body [16]. As shown in Figure 9(a), the tissue phantom consists of 1.8 mm thick skin, 12 mm-thick fat and 15 mm-thick muscle layer. Each layer was designed with frequency dependent dielectric constant (ε_r), conductivity (σ), and loss tangent ($\tan\delta$) values to provide realistic simulation results [17]. The values used at 2.4 GHz and 5.5 GHz are listed in Table 1. The dimension of the phantom used was 150 mm $\times$ 150 mm. The proposed antenna with ground size of 80 mm $\times$ 80 mm was installed on top of the phantom. Figure 9(b) shows the comparison of antenna's S_{11} with and without the phantom. It can be seen that the lower frequency band of 2.45 GHz is less sensitive to the presence of the phantom than the higher frequency band of 5.5 GHz. S_{11} at 5.5 GHz is degraded from -12 dB to -9 dB. In order to compensate this, additional tuning was carried out by

Table 1. Frequency-dependent properties of human tissue.

Tissue	2.45 GHz			5.5 GHz		
	ε_r	σ (S/m)	$\tan\delta$	ε_r	σ (S/m)	$\tan\delta$
Skin (dry)	38.007	1.464	0.283	35.363	3.463	0.320
Fat	5.280	0.105	0.145	4.983	0.274	0.180
Muscle	52.729	1.739	0.242	48.883	4.609	0.308

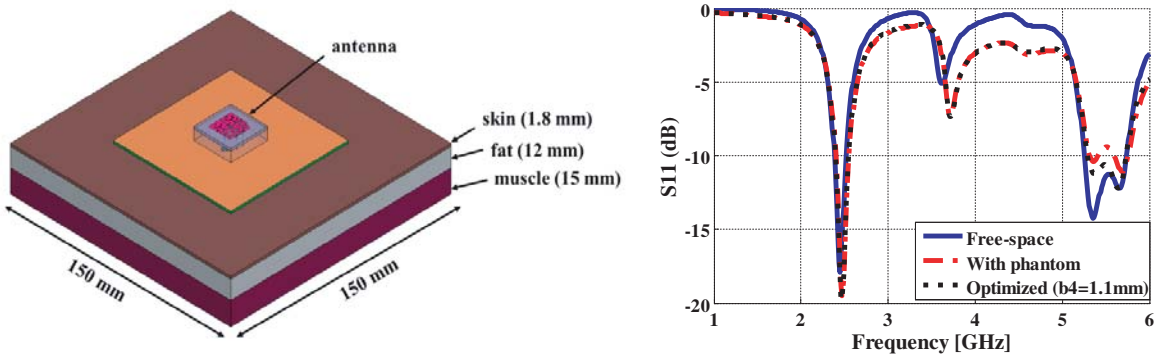

(a) (b)

Figure 9. Influence of human tissue on antenna performance. (a) Simulation model with a three-layer tissue phantom and (b) S_{11} comparison.

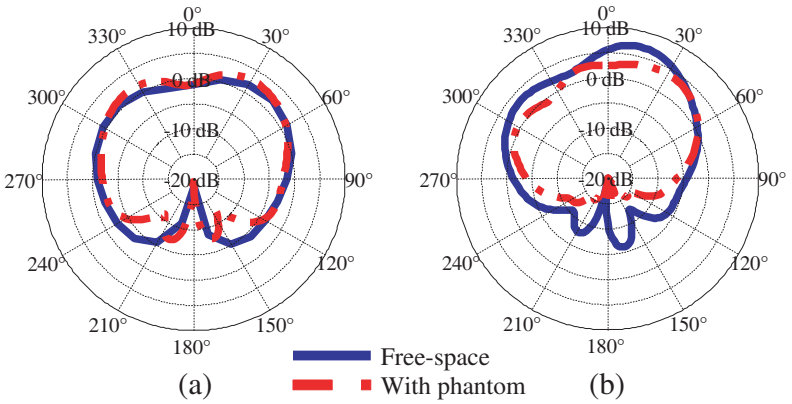

Figure 10. Effects of human phantom on radiation pattern at (a) 2.45 GHz and (b) 5.5 GHz.

tailoring down $b4$ (width of the arm-4, see Figure 1) from 1.2 mm to 1.1 mm. As in Figure 9(b) S_{11} at 5.5 GHz is improved without affecting the lower band.

Reduction of antenna gain was also observed as the antenna is installed on the phantom. The amount of gain reduction was around 0.75 dBi and 2.5 dBi for 2.45 GHz and 5.5 GHz, respectively. The 5.5 GHz was more affected due to higher $\tan\delta$ of the phantom materials. Figure 10 compares the antenna's radiation patterns with and without the phantom. As can be seen, the overall shape of the radiation pattern is maintained except for the broadside gain reduction at 5.5 GHz.

The antenna's far-field radiation characteristics can be used as an indicator to estimate the off-body communication performance at 5.5 GHz band. Nevertheless, it is insufficient to evaluate the on-body communication performance at 2.45 GHz band where its propagation mechanism is mainly through the creeping wave over the body surface [18].

In this regard, we performed a full-wave simulation to investigate path loss between two antennas mounted on a body phantom at 2.45 GHz. Figure 11 illustrates the simulation model. The two antennas are mounted on the front and back of a body phantom. The latter is filled with a homogeneous material to reduce computing effort. The material used is muscle which is the most lossy one among various tissues in human body. With this environment, line of sight communication is impossible due to the high loss and thickness of the phantom; therefore, the resulting S_{21} completely relies on the detour path along the phantom surface. To validate the simulation result, S_{21} measurement was conducted by measuring the path loss between two identical antennas installed on author's chest and abdomen. Figure 12 shows the measured S_{21} compared to simulation result at 2.45 GHz band. The measured result exhibits similar trend to the simulation with the maximum S_{21} value of -32.7 dB at 2.44 GHz. This value is comparable to previous studies using higher-mode microstrip patch antenna [19] and a quarter-wavelength monopole [20].

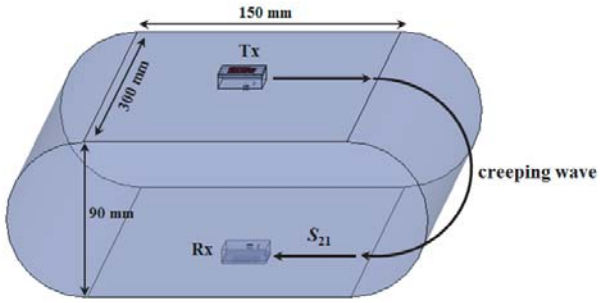

Figure 11. Illustration of on-body coupling simulation.

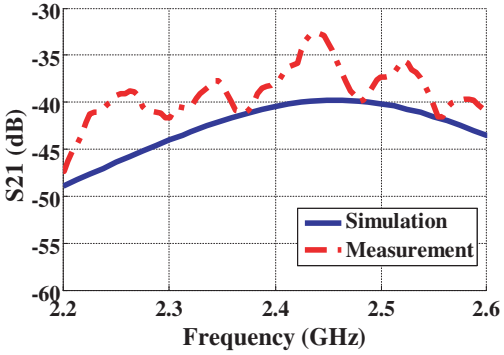

Figure 12. S_{21} coupling of proposed antennas.

5. CONCLUSION

A miniaturized low-profile antenna utilizing a third order Hilbert curve fractal geometry was investigated using full-wave simulations and measurements. The proposed antenna supports pattern diversity at different frequency bands without the use of electrical switches. As a result, it is easy to fabricate in a small footprint. Simulation and measurement results demonstrated that a monopole-like omnidirectional radiation pattern was shown in the 2.45 GHz ISM band, and a patch-like broadside pattern was exhibited in the 5.5 GHz WLAN band. The former is available for on-body communication along horizontal links while the latter is useful for off-body communication. The 5.5 GHz WLAN band has a higher gain and wider bandwidth than the 2.45 GHz band. Thus, it is suitable for sending larger data over a longer distance which matches to off-body communication purpose. The body-worn antenna performance was investigated by means of full-wave simulations. The results showed that the 5.5 GHz high band was vulnerable to the high loss of human body but sufficient to conduct off-body communication. The simulation results of on-body communication at 2.4 GHz also demonstrated considerable performance for body-centric application.

ACKNOWLEDGMENT

This work was supported by The Basic Science Research Program through the National Research Foundation of Korea (NRF) funded by the Ministry of Science, ICT, & Future Planning (No. 2013R1A1A1005735).

REFERENCES

1. Cavallari, R., F. Martelli, R. Rosini, C. Buratti, and R. Verdone, "Survey on wireless body area networks: Technologies and design challenges," *IEEE Comm. Surveys Tutor.*, Vol. 16, No. 3, 1635-1657, Third Quarter, 2014.
2. Li, M., S. Q. Xiao, and B. Z. Wang, "Pattern-reconfigurable antenna for on-body communication," *Proc. IMWS-BIO*, 1–3, 2013.
3. Scott, H. and V. F. Fusco, "Antenna array beam-steering by the integration of a series phase shifter," *Proc. High Freq. Postgrad. Stu. Colloq.*, 25–29, 2001.
4. Yusuf, Y. and X. Gong, "Low-cost patch antenna phased array with analog beam steering using mutual coupling and reactive loading," *IEEE Antennas Wirel. Propag. Lett.*, Vol. 7, 81–84, 2008.
5. Lim, I. and S. Lim, "Monopole-like and boresight pattern reconfigurable antenna," *IEEE Trans. Antennas Propag.*, Vol. 61, No. 12, 5854–5859, Dec. 2013.
6. Lee, S. W. and Y. Sung, "A polarization diversity patch antenna with reconfigurable feeding network," *J. Electromagn. Eng. Sci.*, Vol. 15, No. 2, 115–119, Apr. 2015.
7. Nessel, J. A., A. J. Zaman, and F. A. Miranda, "A miniaturized antenna for surface-to-surface and surface-to-orbiter applications," *Microw. Opt. Tech. Lett.*, Vol. 48, No. 5, 859-862, Mar. 2006.
8. Patel, M. and J. Wang, "Applications, challenges, and prospective in emerging body area networking technologies," *IEEE Trans. Wirel. Commu.*, Vol. 17, No. 1, 80–88, Feb. 2010.
9. Anguera, J., C. Puente, and J. Soler, "Miniature monopole antenna based on fractal Hilbert curve," *Proc. IEEE Antennas Propag. — Soc. Int. Symp.*, Vol. 4, 546–549, 2002.
10. Vinoy, K. J., K. A. Jose, V. K. Varadan, and V. V. Varadan, "Resonant frequency of Hilbert curve fractal antennas," *Proc. Antennas Propag. — Soc. Int. Symp.*, Vol. 3, 648–651, 2001.
11. Azaro, R., F. Viani, L. Lizzi, E. Zeni, and A. Massa, "A monopolar quad-band antenna based on a Hilbert self-affine prefractal geometry," *IEEE Antennas Wirel. Propag. Lett.*, Vol. 8, 177–180, 2009.
12. Sinha, S. N. and M. Jain, "A self-affine fractal multiband antenna," *IEEE Antennas Wirel. Propag. Lett.*, Vol. 6, 110–112, 2007.
13. Mahatthanajatuphat, C., P. Akkaraekthalin, S. Saleekaw, and M. Krairiksh, "A bidirectional multiband antenna with modified fractal slot fed by CPW," *Progress In Electromagnetics Research*, Vol. 95, 59–72, 2009.
14. Wang, Z., L. Z. Lee, D. Psychoudakis, and J. L. Volakis, "Embroidered multiband body-worn antenna for GSM/PCS/WLAN communications," *IEEE Trans. Antennas Propag.*, Vol. 62, No. 6, 3321–3329, Jun. 2014.
15. See, T. S. P. and Z. N. Chen, "Experimental characterization of UWB antennas for on-body communications," *IEEE Trans. Antennas Propag.*, Vol. 57, No. 4, 866–874, Apr. 2009.
16. Christ, A., A. Klingenbock, T. Samaras, C. Goiceanu, and N. Kuster, "The dependence of electromagnetic far-field absorption on body tissue composition in the frequency range from 300 MHz to 6 GHz," *IEEE Trans. Microw. Theory Tech.*, Vol. 54, No. 5, 2188–2195, May 2006.
17. Inst. of Appl. Phys., "Calculation of the dielectric properties of body tissues in the frequency range 10 Hz–100 GHz," Italian Nat. Res. Council, Florence, Italy, [Online] Available: http://niremf.ifac.cnr.it/tissprop/.
18. Ryckaert, J., P. De Doncker, R. Meys, A. de Le Hoye, and S. Donnay, "Channel model for wireless communication around human body," *IEEE Electron. Lett.*, Vol. 40, No. 9, 543–544, Apr. 2004.
19. Conway, G. A. and W. G. Scanlon, "Antennas for over-body-surface communication at 2.45 GHz," *IEEE Trans. Antennas Propag.*, Vol. 57, No. 4, 844–855, Apr. 2009.
20. Hall, P. S., Y. Hao, Y. I. Nechayev, A. Alomainy, C. C. Constantinou, C. Parini, M. R. Kamarudin, T. Z. Salim, D. T. M. Hee, R. Dubrovka, A. S. Owadally, S. Wei, A. Serra, P. Nepa, M. Gallo, and M. Bozzetti, "Antennas and propagation for on-body communication systems," *IEEE Antennas Propag. Mag.*, Vol. 49, No. 3, 41–58, Jun. 2007.